Shape optimization of a disc-pad system under squeal noise criteria

Pradeep Mohanasundaram, Frédéric Gillot, Koji Shimoyama, Sébastien Besset

Shape optimization of a disc-pad system under squeal noise criteria

Pradeep Mohanasundaram[1,2,4,†], Frédéric Gillot[1,3,4,‡], Koji Shimoyama[2,4,⋄], and Sébastien Besset[1,4,*]

[1]LTDS, École Centrale de Lyon, 36 av. Guy de Colongue, 69134 Écully cedex, France

[2]IFS, Tohoku University, Sendai, Japan

[3]INRIA, I4S Team, Campus de Beaulieu, 35000 Rennes, France

[4]ElyTMaX UMi 3757, CNRS, Université de lyon, Tohoku University, international Joint

Unit, Tohoku University, Sendai, Japan

[*]Corresponding author, sebastien.besset@ec-lyon.fr

[†]pradeep.mohanasundaram@ec-lyon.fr

[⋄]shimoyama@tohoku.ac.jp

[‡]frederic.gillot@ec-lyon.fr

1

Abstract

This paper deals with the parametric shape optimization of a simplified model of brake system under squeal noise criteria. As brake squeal phenomenon induces under-quality perception for industrial structures such as cars and trains, its understanding and management are important challenges for future systems design. Hence, we expose an optimization methodology based on meta-model for a proposed computationally expensive stability criteria representing the squeal noise. Sensitivity analysis is first conducted to assess and validate the chosen geometrical parameters. Then, a Pareto front is obtained through optimization of the system, leading to a set of optimal solutions for the considered multi-objective case.

Keywords: vibration, brake squeal, optimization, kriging.

1 Introduction

Brake squeal phenomenon induces under-quality perception for industrial structures such as cars and trains, and its understanding is an important challenge [9, 6, 7, 14, 1, 2]. Understanding squeal noise requires the analysis of brake systems from a "vibration and acoustic" point of view. Though the generation of squeal noise is considered to be a very complex phenomenon with many mathematical models defining in their respective sense, one of the most common methods which is efficiently used in prediction is using the complex eigenvalue analysis, even if it is well known that it can lead to under or over-estimation of unstable modes [17, 10, 16]. The main advantage of this method remains its speed, especially in the context of optimization, where the objective functions have to be evaluated several times.

The aim of this paper is to optimize the shape of a simplified brake system consisting of a pad and a disc, both described through finite element method for evaluation of the proposed criteria through complex eigenvalue analysis. As direct shape optimization using the finite element model for evaluation of the defined criteria would lead to prohibitive calculation costs, the strategy proposed in this paper considers an Efficient Global Optimization (EGO [8]) algorithm. The physical model is represented through a meta-model which is computationally inexpensive, in our case a kriging meta-model [4], on which a meta-heuristic optimistaion is applied, in our case a genetic algorithm (GA) [5]. This coordination of algorithms allows to quickly acquire a set of Pareto optimal solutions to be considered for the choice of the design.

We will introduce the considered brake system model and the constraints used in the second section. The third section will describe the model reduction technique applied in order to reduce the computation time for the dynamical system. In section four, we will introduce the proposed criteria, followed by a short description of the effect of mesh on the criteria in section five. Based on this criteria, sensitivity analysis is performed for the geometrical parameters characterizing the model, which is described in section six. The computation time required for the optimization being very important,

we introduce in section seven, the use of kriging meta-model, before describing the optimization loop in section eight. Results of the cross-validation of the meta-model, the sensitivity analysis and the multi-objective optimization are analysed in section nine and at last we conclude in section ten.

2   Model description

The Figure 1 shows the considered disc-pad model used for the optimization process. The simplified model is proposed since the main objective concerns about optimizing the squeal phenomenon with respect to the fundamental shape parameters in a typical disc brake system. The brake disc is modelled as a disc geometry, where a fixed constraint is applied to the cylindrical inner face of the disc. The brake pad is modelled as a disc sector. The pad model is considered to have one face on contact with the disc while the edges along the other face are constrained to move only along the surface normal of the disc. The relative position between the disc and the pad is constrained to be concentric.

[Figure 1 about here.]

2.1   Contact law

The contact characteristic between the disc and the pad for conforming mesh at the contact interface is modelled using Node-to-Node contact with massless spring elements, enforcing the condition of no separation at the interface. This can be viewed as contact using the penalty method, but without the need for the applied force, since the main interest only concerns the dynamical interaction with respect to squeal noise; the instability causing the squeal noise is considered to be due to the phenomenon of mode coalescence induced by friction, which can be captured by modal analysis of the system in its steady-state. Hence, the given contact definition represents the dynamics at the interface through spring elements of certain stiffness. Further reference to the use of this type of contact in detail can be found in [19] and the review article [14]. The contact force using the spring element is defined by linear contact stiffness as shown below.

$$F_{cont} = K_l(x_d - x_p) \tag{1}$$

where K_l represents the linear contact stiffness and $(x_d - x_p)$ represents the relative displacement between a contact node of the disc and the corresponding contact node of the pad.

The contact definition directly relates to the definition of friction which in turn dictates the stability criteria considered for optimization. Hence the influence of the variation of the contact stiffness should be reduced in effecting the stability criteria with respect to the shape parameters during optimization, which leads to the definition of global contact stiffness K_{Gl}. Global contact stiffness is chosen to be independent of the dimensions of the contact interface, and the contact stiffness between any two corresponding contact nodes is defined by local contact stiffness K_l. The global contact stiffness is hence defined as a

2

constant and a multiple of local contact stiffness, depending on the number of pairs of contact nodes at the interface n.

$$K_{Gl} = K_l \times n \tag{2}$$

The global contact stiffness K_{Gl} is chosen considering the numerical stability with respect to the eigenvalue analysis. Further the convergence of the stability criteria for a given design point based on the choice of the number of contact pairs is also discussed in section 5.

2.2 Friction law

The classic Coulomb's law of friction is considered to define the friction characteristics. The steady state condition to describe the friction force $\mathbf{F_{fric}}$ is considered to be product of the coefficient of friction μ and the normal force $\mathbf{F_{cont}}$ as defined in the previous section and hence the friction force $\mathbf{F_{fric}}$ is given as follows:

$$\mathbf{F_{fric}} = \mu \mathbf{F_{cont}} \tag{3}$$

Hence the effect of friction is modeled at the interface through the relative displacement $(x_d - x_p)$ of the contact pairs of nodes, making it in a also sense suitable for modal analysis in relation to contact conditions. With respect to the motion of the disc, the friction force can be resolved in to tangential and radial directions. The relative sliding velocity is negligible in the radial direction and hence the friction effects from the radial direction is also negligible and hence, ignored to simplify the model. The net effect of friction is described with the dot product of unit tangential vector v_t at a given node of disc, as follows:

$$\mathbf{F_{fric.disc}} = \mu \mathbf{F_{cont}}.v_t \tag{4}$$

The reaction force $\mathbf{F_{fric.pad}}$ on the pad of the above friction component $\mathbf{F_{fric.disc}}$ can be similarly defined as negative of $\mathbf{F_{fric.disc}}$.

2.3 Description of the system

The equation describing the dynamics of the system in steady-state is given as follows.

$$\mathbf{M\ddot{U}} + \mathbf{C\dot{U}} + (\mathbf{K} + \mathbf{K_f})\mathbf{U} = \mathbf{0} \tag{5}$$

where $\mathbf{M}$ and $\mathbf{C}$ represents the mass and the damping matrices respectively for the system. $\mathbf{K}$ represents the stiffness matrix of the system with the contact definition, described as mentioned in the subsection 2.2 and $\mathbf{K_f}$ is the friction definition, defined as described in the subsection 2.3. $\mathbf{U}$ is the vector representing the degrees of freedom of the system, and its subsequent derivatives denoted with overdots.

2.4 Parameters description and range

Table 1 shows the parameters used to build the finite element model and the permitted variations of the shape variables.

[Table 1 about here.]

3 Model Reduction

The evaluation of the stability criteria involves expensive computation for eigenvalues evaluated at various friction coefficients to capture the evolution of the instability. While only the major unstable modes constituting the squeal noise is required to be identified, the model can be simplified by dynamic model reduction techniques. This further allows us to simplify the damping definition of the dynamic model with the method of modal damping. The method of Craig & Bampton reduction is applied to the model, which is considered to be effective since it captures the dynamic properties at the contact interface and also the internal dynamic properties of the models involved in contact. More detailed description of Craig & Bampton method used in brake squeal application can be found in literature [3] and [12]. In accordance with the Craig & Bampton theory, the vector $\mathbf{U}$ and the matrices $\mathbf{K}$ and $\mathbf{M}$ are split between internal and interface degrees of freedom as follows:

$$\mathbf{U} = \left\{ \begin{array}{c} \mathbf{U}_i \\ \mathbf{U}_j \end{array} \right\}; \quad \mathbf{K} = \left[\begin{array}{cc} \mathbf{K}_{ii} & \mathbf{K}_{ij} \\ \mathbf{K}_{ji} & \mathbf{K}_{jj} \end{array} \right]; \quad \mathbf{M} = \left[\begin{array}{cc} \mathbf{M}_{ii} & \mathbf{M}_{ij} \\ \mathbf{M}_{ji} & \mathbf{M}_{jj} \end{array} \right] \tag{6}$$

where $\mathbf{U_i}$ and $\mathbf{U_j}$ are internal and interface degrees of freedom respectively. The transformation matrix $\mathbf{T}$ is defined as composition of static transformation $\boldsymbol{\Phi}_s$ and Eigen vectors $\boldsymbol{\Phi}_d$, as follows.

$$\mathbf{T} = \left[\begin{array}{cc} \boldsymbol{\Phi}_d & \boldsymbol{\Phi}_s \\ \mathbf{0} & \mathbf{I} \end{array} \right]; \quad \boldsymbol{\Phi}_s = \mathbf{K}_{ii}^{-1} \mathbf{K}_{ij}; \quad \boldsymbol{\Phi}_d = [\Phi_0, \Phi_1, ..., \Phi_n] \tag{7}$$

where Φ_n is the nth eigenvector obtained from the eigenvalue problem defined as $(\mathbf{K}_{ii} - \omega_n^2 \mathbf{M}_{ii})\Phi_n = 0$. The choice of the number of eigenvectors n considered for reduction depends on the convergence required with respect to prediction of the eigenvalues for the unstable modes obtained by the reduced model.

The reduced mass matrix $\mathbf{M}_r$ and stiffness matrix $\mathbf{K}_r$ are respectively obtained through the transformation matrix $\mathbf{T}$ applied as $\mathbf{T}^t \mathbf{M}_s \mathbf{T}$ and $\mathbf{T}^t \mathbf{K}_s \mathbf{T}$, where $\mathbf{K}_s$ is the stiffness matrix of the system with friction definition. The matrix $\mathbf{K}_r$ is largely uncoupled, defined in the modal coordinates, except for the non-diagonal terms which can be viewed as the terms constituting the effects of friction in the modal coordinates and also the part of the matrix with static reduction is non-diagonal. While the reduction of the mass matrix from $\mathbf{M}_s$ to $\mathbf{M}_r$ is simply straight forward.

The Craig-Bampton reduction leads to reduced matrices of size $[\,\mathbf{S} \times \mathbf{S}\,]$, where $\mathbf{S}$ is given by the sum of the number of contact points at the system interface and the number of eigenvectors of the

4

system considered. This greatly reduces the computation time of the Complex eigenvalue analyses for the estimation of the stability criteria.

4   Stability criteria

The transient numerical model used to describe the braking phenomenon is highly non-linear and very unrealistic to be used for optimisation. Hence, the characteristic equation of the eigenvalue problem for the system 5 is described as follows.

$$(\lambda^2 \mathbf{M} + \lambda \mathbf{C} + (\mathbf{K} + \mathbf{K_f}))\mathbf{\Phi} = \mathbf{0} \tag{8}$$

where λ is an eigenvalue and $\mathbf{\Phi}$ its corresponding eigenvector of the system. When the above model is expressed in the state-space form, the Lyapunov stability conditions can be used to describe the stability of the system around the considered steady-state. Without the effect of friction, the asymptotic stability of the system in the presence of damping leads to all negative real parts for the complex eigenvalues. While the presence of instability due to friction is given by at least one or many complex eigenvalues with positive real part for the system, which is considered to cause the instability inducing the squeal noise.

Considering a multi-objective problem, the stability criteria has to be a scalar C_s representing the presence and perceived level of squeal noise. We propose the formulation of equation 9 when $X \approx \mathcal{N}(\bar{X}, \sigma)$:

$$C_s = \int_\mu \max\{\Re(f(X))\} \tag{9}$$

where μ represents the disc-pad friction coefficient, and $f(X)$ represents the complex solutions (eigenvalues) of the dynamical eigenvalue problem 8. The robust optimization requires to consider uncertain parameters. The deterministic optimization corresponds to $\sigma = 0$ for the given description.

The minimization of the proposed criteria defines the minimization of the brake squeal noise with respect to the structure of the brake system irrespective of the friction coefficient. This is important since the squeal noise can be easily reduced by reducing the friction coefficient but defying the main objective of the braking, and this importance of friction coefficient compared to the material parameters in relation to instability is shown with sensitivity analysis by Nechak et al [13] where similar criteria is considered. Thus the minimization of the criteria with respect to the shape parameters represents the least possibility or lower magnitude of the squeal noise for a given range of parameters.

The evaluation of this type of criteria is computationally expensive but can be made possible with parallel computation, thus evaluating $Max\{\Re(f(X))\}$ in parallel for a regular interval of $\delta\mu$ at once and

hence defining the criteria as follows.

$$\int_\mu Max\{\Re(f(X))\} = \lim_{\delta\mu\to 0} \sum_{\mu=0}^{1} Max\{\Re(f(x,\mu))\}\delta\mu \qquad (10)$$

For convenience the stability criteria is scaled to be defined as an integer and the absence of instability is given by values less than zero due to the absence of the positive real part. The histogram of the stability criteria for the design points from latin hypercube sampling within the design space from range in table 1 is given as follows.

[Figure 2 about here.]

As it can be seen, most of the design points show very high instability with maximum distribution around 450 to 550, and with only very few design points contributing to values less than 100.

5   Mesh vs Stability criteria comparison

In relation to the expensive evaluation of the stability criteria, convergence study was performed to reduce the total degrees of freedom in the system and the influence of the number of contact points on the variance of the stability criteria. The eigenmodes which causes maximum instability as predicted by the maximum positive real part of the complex eigenvalues are only of interest to us and hence, taken in to account to check for convergence.

5.1   Mesh outside of the contact interface

The dynamic properties with respect to considered maximum instability show little variation for change in mesh size out of the contact region for given shape parameters and number of contact points. The comparison is shown through a model with highly coarse mesh as in figure 3 against a model of same shape parameters but with a relatively fine mesh as in figure 4 while maintaining the same number and position for the contact points. The mismatch in frequencies between the models is shown in figure 5 where the range for frequency is zoomed to the frequencies which induce mode coalescence predicted to cause the maximum instability. The shift in unstable frequencies and the point of bifurcation of the maximum real part as shown in figure 6 are observed to be very low relative to the change in mesh size.

[Figure 3 about here.]

[Figure 4 about here.]

[Figure 5 about here.]

[Figure 6 about here.]

5.2 Mesh at the contact interface

Though the variation of the mesh out of the contact interface is shown to have a little influence, the variation of the mesh at the contact interface is observed to have a considerable effect on the dynamic properties. This can be seen by comparing results of the models in figure 3 and figure 4 against the models in figure 7 and figure 8 which are of the same shape parameters. Hence, it is intuitive to assume a large number of contact points to explain the instability, confirming as possible to reality. The convergence is shown through varying but large number of contact points as in figure 7 and 8 with plot for bifurcation of the real part (figure 10) and frequencies inducing maximum instability (figure 9).

[Figure 7 about here.]

[Figure 8 about here.]

[Figure 9 about here.]

[Figure 10 about here.]

5.3 Meshing strategy

The definition of the contact points is observed to have a significant influence on the maximum real part of the complex eigenvalues and hence, the stability criteria. Hence, proper mesh definition is seen as important considering the computation cost. This leads to the definition of mesh as in figure 11 where linear hexahedral elements are largely used through out the model with smaller elements at the contact interface and the region outside of contact interface is defined by larger elements. The difference in mesh density is compromised by introducing 3D wedge elements to maintain a structured mesh. This is considered to greatly reduce the time for simulation while reducing the uncertainties in the stability criteria induced by choice of the number of contact points.

[Figure 11 about here.]

6 Methods

6.1 Sensitivity analysis

The global sensitivity analysis for the involved shape parameters was performed using the Variance-based method which comes from Hoeffding-Sobol decomposition [18]. This method is based on decomposing the variance of a function to its variance associated with the parameters and the interaction between the parameters. Hence, higher the variance in output of a function induced by a parameter infers higher its sensitivity. The method is applied through Monte-Carlo based estimation defined by latin hypercube

sampling for efficiency. In effect, to evaluate the global behaviour and to increase the accuracy for the given Monte-Carlo based estimation on the presumed asymptotic case demands a large computation of design points, which is simply impossible to converge with a reasonable time given the computation cost to evaluate the stability criteria. Hence, a surrogate model based on kriging is used, which is described in detail in section 6.2. The stability criteria given by surrogate model is defined as $\hat{C}_s$, where $C_s \approx \hat{C}_s$.

To understand the effect of the shape parameters on the stability criteria, the first-order and the total-order sensitivity indices are computed. The first-order indices defines the contribution of a given parameter to the change in unconditional variance $V(\hat{C}_s)$, while the total-order indices adds to it the contribution of all the higher-order interactions on the given parameter. The general definition of the first-order index S_i and the total-order index S_{Ti} are given as follows.

$$S_i = \frac{V_{X_i}(E_{X_{\sim i}}(\hat{C}_s|X_i))}{V(\hat{C}_s)} \tag{11}$$

$$S_{Ti} = 1 - \frac{V_{X_{\sim i}}(E_{X_i}(\hat{C}_s|X_{\sim i}))}{V(\hat{C}_s)} \tag{12}$$

where $V_{X_i}(E_{X_{\sim i}}(\hat{C}_s|X_i))$ is the variance of the conditional expectation on the function of the stability criteria $\hat{C}_s$ evaluated by conditioning the parameter X_i for several values across the bounded design space and similarly, $V_{X_{\sim i}}(E_{X_i}(\hat{C}_s|X_{\sim i}))$ is the variance of the conditional expectation obtained by conditioning all parameters except for X_i.

The described probability measures are estimated based on the estimators proposed in [11]. The Monte-Carlo based estimation for the given estimators require two matrices Y_A and Y_B of equal size with rows and columns representing the design points and the parameters respectively, defined by latin hypercube sampling. To evaluate the first order index of the ith parameter, all the parameters of Y_B are unchanged except for the ith parameter (ith column of the matrix) which is replaced by the ith parameter of Y_A to obtain the matrix Y_{Bi}. Similarly, for evaluation of the total-order index of the ith parameter, all the parameters of Y_B are changed with the parameters of Y_A except for the ith parameter to obtain the matrix Y_{Bti}. Hence, the matrices Y_{Bi} and Y_{Bti} represent the conditioning of the parameters w.r.t. the matrix Y_A, which in a sense is used to evaluate the conditional probability terms and also to describe the effective unconditional variance, as given by the estimators. For n parameters and p design points where the parameters are to be conditioned, it requires an estimation of $(n+1)p$ design points to evaluate the first order index or the total order index of all the parameters.

6.2 Kriging meta-model

When dealing with meta-modeling, several approaches are available. We will focus here on methods without a-priori function basis selection, i.e. fitting observations with given orthogonal basis functions. The

EGO [8] approach relies on kriging meta-model, which was well suited in our case for the optimization. Many references are available to deeply understand and study the kriging meta-model [4, 15]. Below, we will limit our description to a brief explanation. Let us consider a physical phenomenon, represented as $Z(\boldsymbol{s})$, where Z is a scalar and $\boldsymbol{s}$ is a vector of inputs :

$$Z(\boldsymbol{s}) = \mu + \delta(\boldsymbol{s}) \tag{13}$$

where μ is an unknown constant and $\delta(\boldsymbol{s})$ an intrinsic stationary (IS) or a second-order stationary (SOS) process. For a given point $\boldsymbol{s}_0$, and considering a set of n observations $(\boldsymbol{s}_0 \ldots \boldsymbol{s}_n)$, we are looking for the least squared prediction error $MSE[\hat{Z}(\boldsymbol{s}_0)] = E[\hat{Z}(\boldsymbol{s}_0) - Z(\boldsymbol{s}_0)]^2$ which leads to $MSE[\hat{Z}(\boldsymbol{s}_0)] = E([\hat{Z}(\boldsymbol{s}_0) - E[Z(\boldsymbol{s}_0)|\boldsymbol{Z}_n]]^2) + E(E[Z(\boldsymbol{s}_0)|\boldsymbol{Z}_n] - Z(\boldsymbol{s}_0)^2)$, such that $min MSE \implies \hat{Z}(\boldsymbol{s}_0) = E[Z(\boldsymbol{s}_0)|\boldsymbol{Z}_n]$ which is impossible to reach practically.

The idea is then to consider $\hat{Z}(\boldsymbol{s}_0)$ as the best linear function of the observed values: $\hat{Z}(\boldsymbol{s}_0) = \sum_{i=1}^n \lambda_i Z(\boldsymbol{s}_i)$, with $\sum_{i=1}^n \lambda_i = 1$ (unbiased condition). Then, defining the $MSE[\hat{Z}(\boldsymbol{s}_0)]$ implies, relying on the variogram function $\gamma_{ij} = \gamma(\boldsymbol{s}_i - \boldsymbol{s}_j)$, such that $\sum_{j=1}^n \lambda_j \gamma_{ij} + \frac{m}{2} = \gamma(\boldsymbol{s}_0 - \boldsymbol{s}_i)$. This can be written as $\boldsymbol{\Gamma\lambda} = \boldsymbol{\gamma}$, leading to find $\boldsymbol{\lambda} = \boldsymbol{\Gamma}^{-1}\boldsymbol{\gamma}$, where $\boldsymbol{\Gamma}$ is usually invertible to reach the predictor $\hat{Z}(\boldsymbol{s}_0) = \sum_{i=1}^n \lambda_i Z(\boldsymbol{s}_i)$. Unfortunately the variogram function (for the IS processes, or the covariance function for the SOS processes, as $2\gamma(\boldsymbol{h}) = 2[C(\boldsymbol{0}) - C(\boldsymbol{h})])$ is unknown and need to be estimated from the data. Therefore, we will consider only the SOS processes, which are more interpretable than the IS processes.

If we assume that all covariances are isotropic, i.e. covariance between two locations depends only on the distance between them, and not on the direction, then $\boldsymbol{C}(\boldsymbol{h}) = \boldsymbol{C}^*(\|\boldsymbol{h}\|)$, with $\|.\|$, a L_2 norm and $\boldsymbol{C}^*(.)$, a function of a scalar variable which represents a parametric covariance function. We have used the classical Matern5/2 covariance structure,

$$C_\nu(h) = \sigma^2 \frac{2^{1-\nu}}{\Gamma(\nu)} \left(\sqrt{2\nu}\frac{h}{\rho} \right)^\nu K_\nu \left(\sqrt{2\nu}\frac{h}{\rho} \right) \tag{14}$$

where, ρ and ν are the non-negative hyper-parameters of this covariance, with Γ representing the Gamma function and K_ν, the modified Bessel function of the second kind.

We reach the optimal hyper-parameters through the classical Maximun Likelihood Estimators (MLEs). It is important to notice that the assumption of Gaussian observations is then very strong.

6.3 Optimization loop

The optimization with respect to only the stability criteria may lead to unworthy designs, mainly with respect to surface area of braking and hence, second objective for optimization was considered to maximise

9

the surface area of contact between the pad and the disc. We used NSGA-II genetic algorithm [5] to obtain a set of Pareto optimal solutions for the multi-objective case without the need of gradient knowledge. This algorithm is used jointly with the kriging meta-model of the stability criteria, to decrease the computation time needed to reach a stable Pareto front. As a stochastic algorithm, the NSGA-II does not require a high level of accuracy to move towards the optimal regions of the design space when the objective functions are smooth enough.

7 Results

The kriging model for the stability criteria is built with 375 design points through latin hypercube sampling from the design space as in 1. The kriging quality check was performed by leave-one-out cross validation and the results are given as follows.

[Figure 12 about here.]

A plot of standardized residuals and a histogram for distribution of errors are also given as follows.

[Figure 13 about here.]

[Figure 14 about here.]

The above analyses show satisfactory results on the quality of the meta-model to be considered for use in expensive computation pertaining to sensitive analysis and for optimisation.

8 Discussion

8.1 Sensitivity analysis

The sensitivity analysis was performed on seven shape parameters as in table 1 describing the complete geometry of the considered model. The value of p as described in section 6.1 is chosen to be 1500 and hence evaluating a total of 24000 design points with meta-model to evaluate the first-order and the total-order indices. The evaluation was repeated for different sample sets to check for convergence, which is seen to be not difficult with the chosen p value and with an estimated standard error for the indices of no more than 0.02.

[Figure 15 about here.]

[Figure 16 about here.]

The description of the parameters are as in 1.

As it can be seen, the first-order indices show relatively high values for the parameters X1 - thickness of the disc and X4 - thickness of the pad. The total-order indices also increase relatively for the two

parameters. But the global variance of the stability criteria can be largely attributed to independent effects from the parameters rather than interaction between them.

Further, the results are also shown with closed second-order indices, combining the independent effects and the interaction between any two parameters.

[Figure 17 about here.]

8.2 Optimal designs

The optimization was considered for the parameters as in sensitivity analysis. The Pareto optimal solutions obtained are shown in figure 18. The optimization was performed on the kriging meta-model 6.2 for minimization of the stability criteria and inverse of the measure of pad surface, to find the course towards minimizing the dynamic instabilities while maximizing the area of contact. The parameters for the genetic algorithm was set to run with a population size of 50 for 25 generations, which was noticed enough to obtain a stable pareto front.

[Figure 18 about here.]

The results from three distinct locations on the Pareto front are shown in the table below.

[Table 2 about here.]

The mid point on the Pareto front shows the balance between the two objectives as a more effective design consideration — while the clear choice of the design can only be considered with more detailed description of the problem surrounding the application.

9 Conclusion

In this paper, the shape optimization using parameters of a simplified brake system under a vibro-acoustic criteria was investigated. In order to reduce the computation cost, a meta-model was first constructed using the kriging theory. The resulting model was able to reproduce the brake squeal phenomenon with good results, and was considered to conduct the optimization process of the system. The optimization was performed using a classical genetic algorithm, providing a Pareto front to represent the optimal solutions of the problem. The optimization scheme used in this paper requires the disc-pad system to be geometrically represented by simple geometrical parameters, thus leading to equally shaped systems. The next step will be to consider the topological representation of the pad, for example with Isogeometric formulation, enabling drastic change in shape and better coverage of the design space.

10 List of abbreviations

IS: Intrinsic Stationary

SOS: Second-Order Stationary

GA: Genetic Algorithm

NSGA: Non-Sorting Genetic Algorithm

EGO: Efficient Global Optimization

11 Declarations

11.1 Avaibility of data and supporting materials

Please contact author for data requests.

11.2 Competing interests

The authors declares that they have no competing interests.

11.3 Fundings

11.4 Author's contributions

P. Mohanasundaram built the FE model and launched the calculations. The content of this paper is part of his PhD work. F. Gillot, K. Shimoyama and S. Besset are the supervisors of Pradeep Mohanasundaram PhD. F. Gillot is involved in the optimization technique used in the paper. K. Shimoyama is involved in the use of the kriging metamodelization. S. Besset is involved int the FE model as well as the structural dynamics analysis of the structure. All authors have read and approved the final manuscript.

11.5 Acknowledgement

References

[1] Ali Belhocine, abd rahim abu bakar, and Oday Abdullah. Structural and contact analysis of disc brake assembly during single stop braking event. *Transactions of the Indian Institute of Metals*, 68:403–410, 06 2015.

[2] Ali Belhocine and Nouby Ghazaly. Effects of material properties on generation of brake squeal noise using finite element method. *Latin American Journal of Solids and Structures*, 12:1432–1447, 06 2015.

[3] S. Besset and J.-J. Sinou. Modal reduction of brake squeal systems using complex interface modes. *Mechanical Systems and Signal Processing*, 85:896 – 911, 2017.

[4] Noel Cressie. The origins of kriging. *Mathematical Geology*, 22(3):239–252, Apr 1990.

[5] K. Deb, A. Pratap, S. Agarwal, and T. Meyarivan. A fast and elitist multiobjective genetic algorithm: Nsga-ii. *IEEE Transactions on Evolutionary Computation*, 6(2):182–197, April 2002.

[6] R.A. Ibrahim. Friction-induced vibration, chatter, squeal, and chaos part 1: mechanics of contact and friction. *Am Soc Mech Eng Appl Mech Rev*, 47(7):209–226, 1994.

[7] R.A. Ibrahim. Friction-induced vibration, chatter, squeal, and chaos part 2: dynamics and modeling. *Am Soc Mech Eng Appl Mech Rev*, 47(7):227–263, 1994.

[8] Donald R. Jones, Matthias Schonlau, and William J. Welch. Efficient global optimization of expensive black-box functions. *Journal of Global Optimization*, 13(4):455–492, Dec 1998.

[9] N.M. Kindkaid, O.M. O'Reilly, and P. Papadopoulos. Automative disc brake squeal. *Journal of Sound and Vibration*, 267:105–166, 2003.

[10] F. Massi, L. Baillet, O. Giannini, and A. Sestieri. Brake squeal: Linear and nonlinear numerical approaches. *Mechanical Systems and Signal Processing*, 21(6):2374 – 2393, 2007.

[11] Hervé Monod, C Naud, and David Makowski. Uncertainty and sensitivity analysis for crop models. *Working with Dynamic Crop Models*, pages 55–100, 01 2006.

[12] M. Monteil, S. Besset, and J.-J. Sinou. A double modal synthesis approach for brake squeal prediction. *Mechanical Systems and Signal Processing*, 70-71:1073 – 1084, 2016.

[13] L. Nechak, F. Gillot, S. Besset, and J.-J. Sinou. Sensitivity analysis and kriging based models for robust stability analysis of brake systems. *Mechanics Research Communications*, 69:136 – 145, 2015.

[14] H. Ouyang, W. Nack, Y. Yuan, and F. Chen. Numerical analysis of automative disc brake squeal : a review. *International Journal of Vehicle Noise and Vibration*, 1:207–231, 2005.

13

[15] Pramudita Satria Palar and Koji Shimoyama. On efficient global optimization via universal kriging surrogate models. *Structural and Multidisciplinary Optimization*, 57(6):2377–2397, Jun 2018.

[16] S. Oberst and J.C.S. Lai. Statistical analysis of brake squeal noise. *Journal of Sound and Vibration*, 330(12):2978–2994, 2011.

[17] J.-J. Sinou, A. Loyer, O. Chiello, G. Mogenier, X. Lorang, F. Cocheteux, and S. Bellaj. A global strategy based on experiments and simulations for squeal prediction on industrial railway brakes. *Journal of Sound and Vibration*, 332(20):5068 – 5085, 2013.

[18] I.M Sobol′. Global sensitivity indices for nonlinear mathematical models and their monte carlo estimates. *Mathematics and Computers in Simulation*, 55(1):271 – 280, 2001. The Second IMACS Seminar on Monte Carlo Methods.

[19] K. Soobbarayen, S. Besset, and J-.J. Sinou. A simplified approach for the calculation of acoustic emission in the case of friction-induced noise and vibration. *Mechanical Systems and Signal Processing*, 50-51:732 – 756, 2015.

14

List of Figures

Figure 1: Representation of the considered brake system in finite element modeling
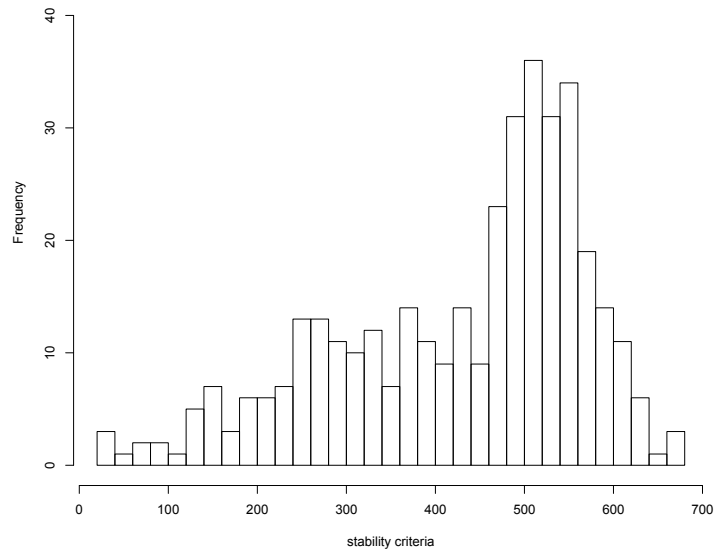
Figure 2: Histogram of the instabilities defined by stability criteria of the design points from latin hypercube sampling of the design space
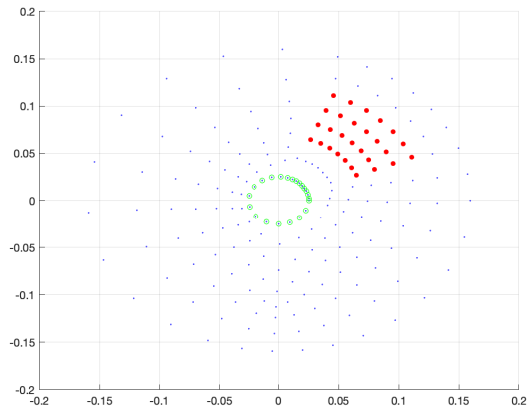
Figure 3: Node plot for a coarse mesh of the disc geometry with contact nodes represented in red
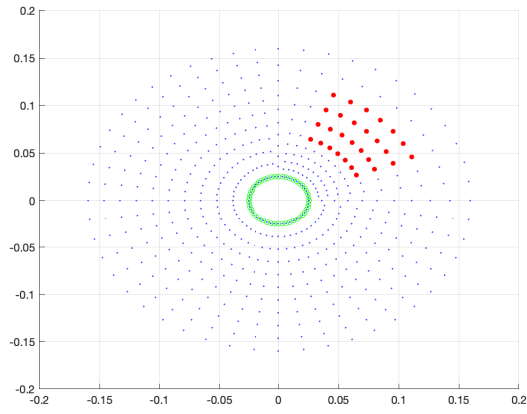
Figure 4: Node plot for a relatively fine structured mesh of the disc geometry with contact nodes represented in red
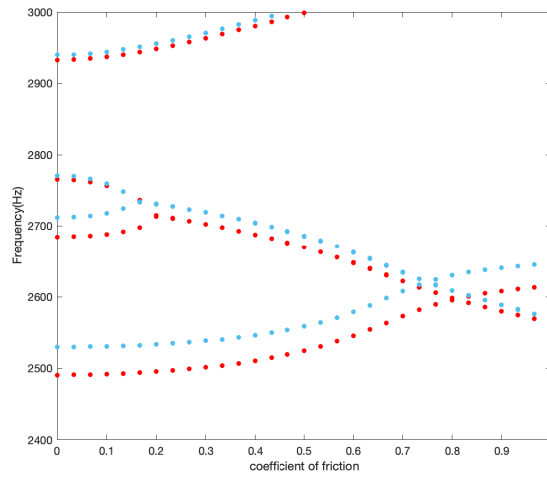
Figure 5: Plot of Frequency vs Friction coefficient, of modes showing maximum instability; Blue represents for the model in 3; Red represents for the model in 4
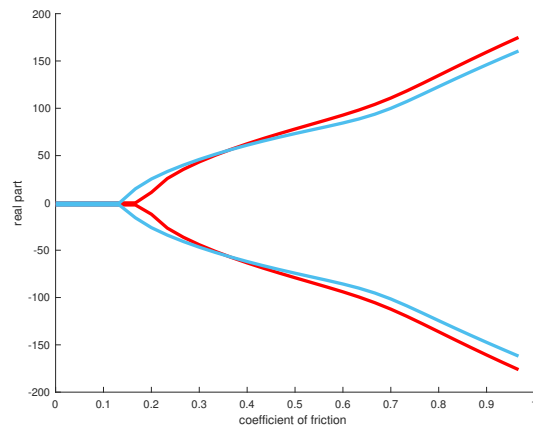
Figure 6: Plot of Real part of the complex eigenvalues vs Friction coefficient, of modes showing maximum instability; Blue represents for the model in 3; Red represents for the model in 4
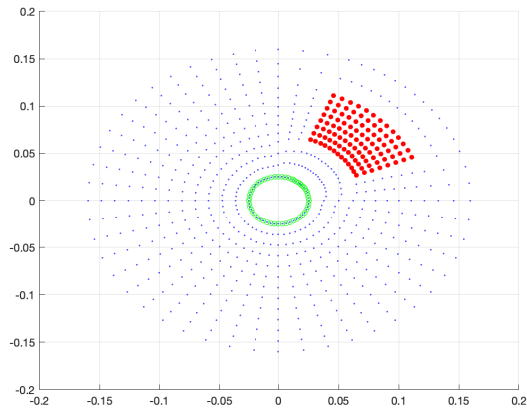
Figure 7: Node plot for a fine mesh with contact nodes represented in red
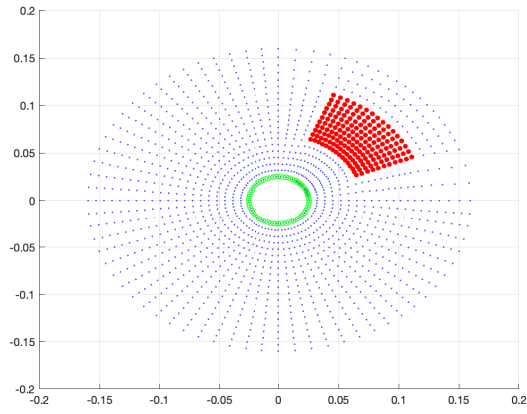
Figure 8: Node plot for a relatively finer mesh compared to 7, especially on the contact interface with contact nodes represented in red
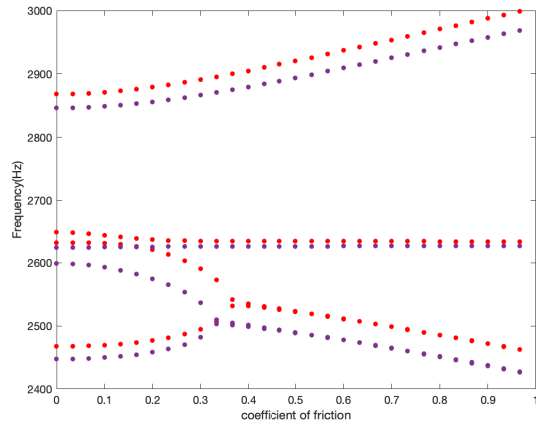
Figure 9: Plot of Frequency vs Friction coefficient, of modes showing maximum instability; Red represents the plot for the model in 7. Violet represents the plot for the model in 8
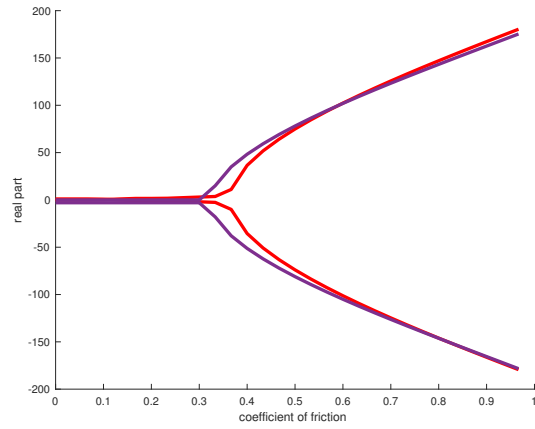
Figure 10: Plot of Real part of the complex eigenvalues vs Friction coefficient, of modes showing maximum instability; Red represents the plot for the model in 7, Violet represents the plot for the model in 8
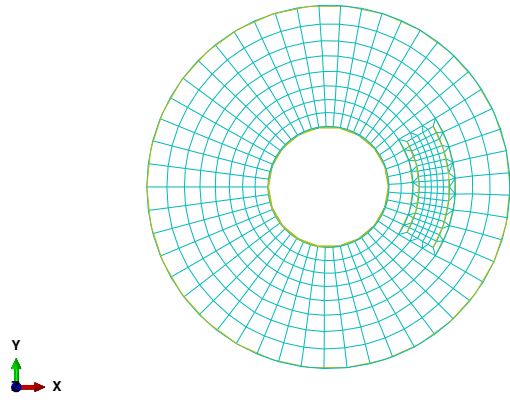
Figure 11: Considered mesh definition
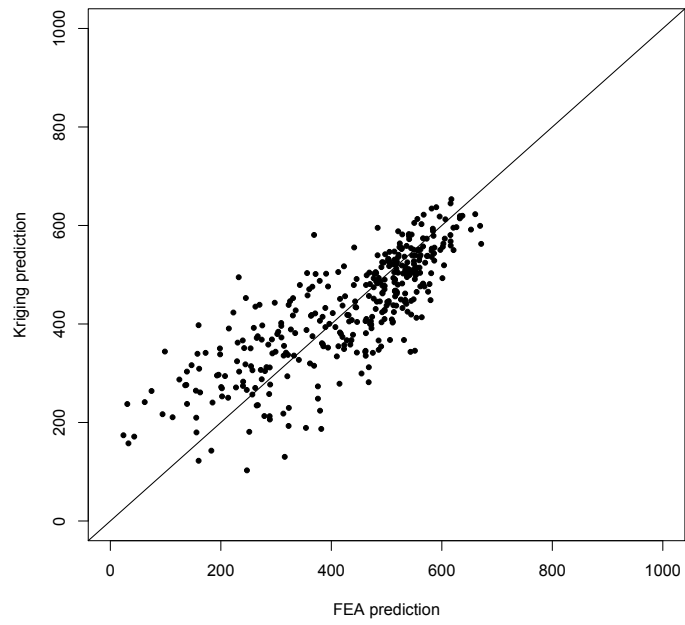
Figure 12: Leave-One-Out Cross-validation
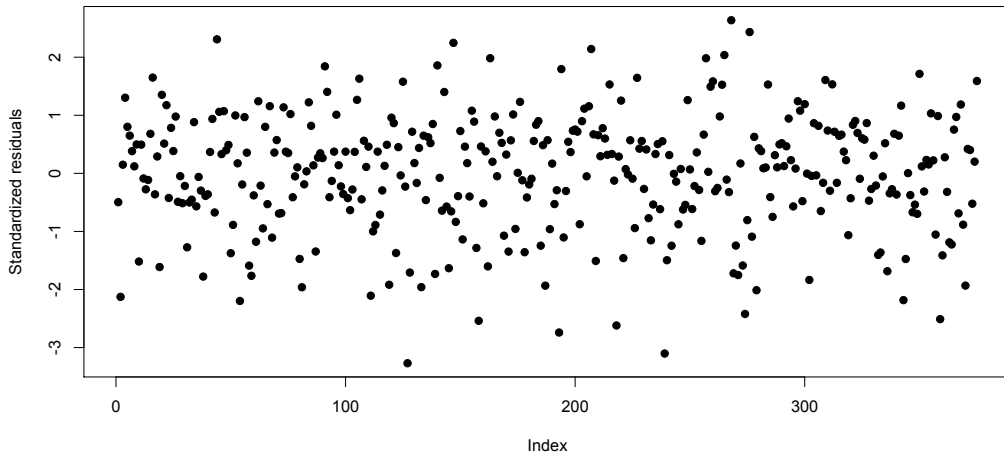
Figure 13: Standardized residuals from leave-One-Out Cross-validation
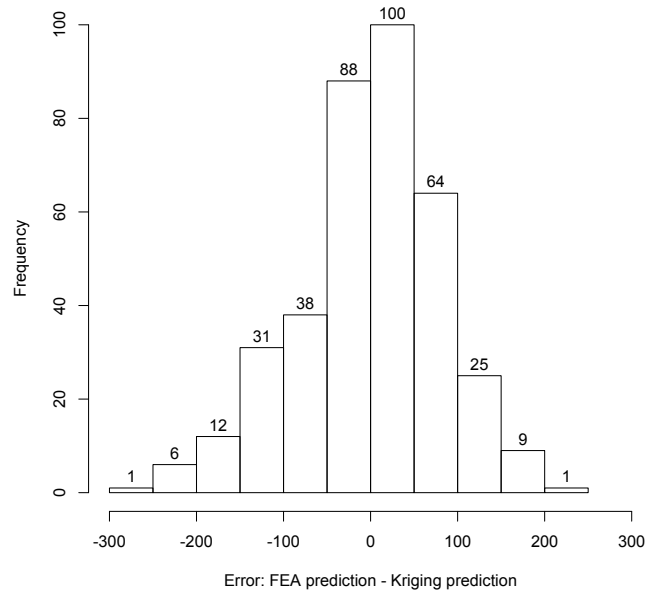
Figure 14: Histogram of the distribution of error
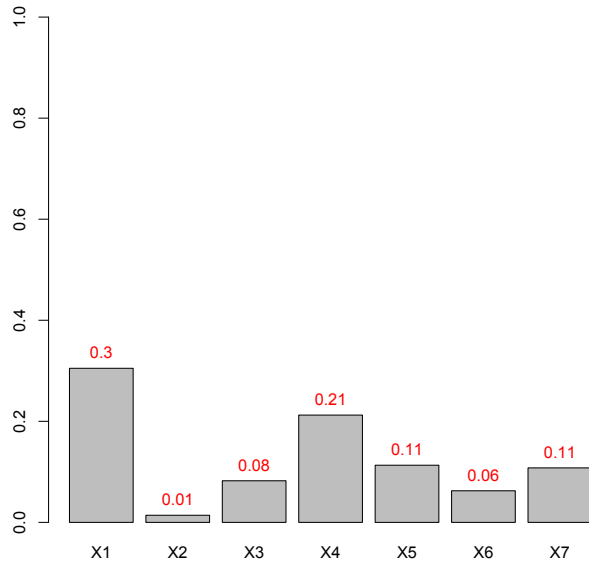
Figure 15: First-order Sobol indices
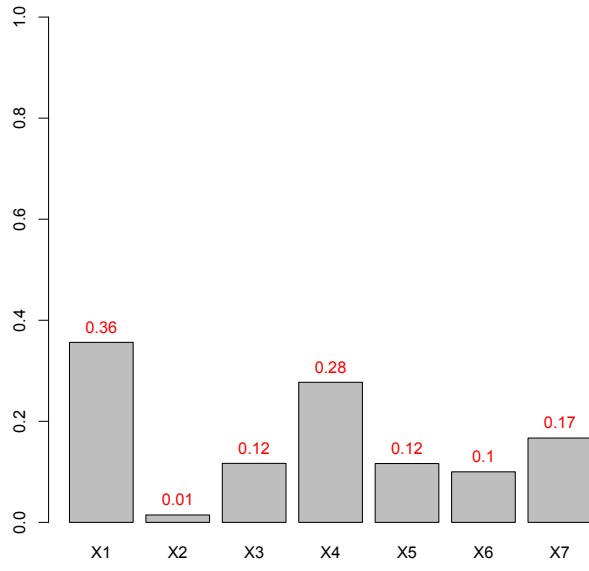
Figure 16: Total-order Sobol indices
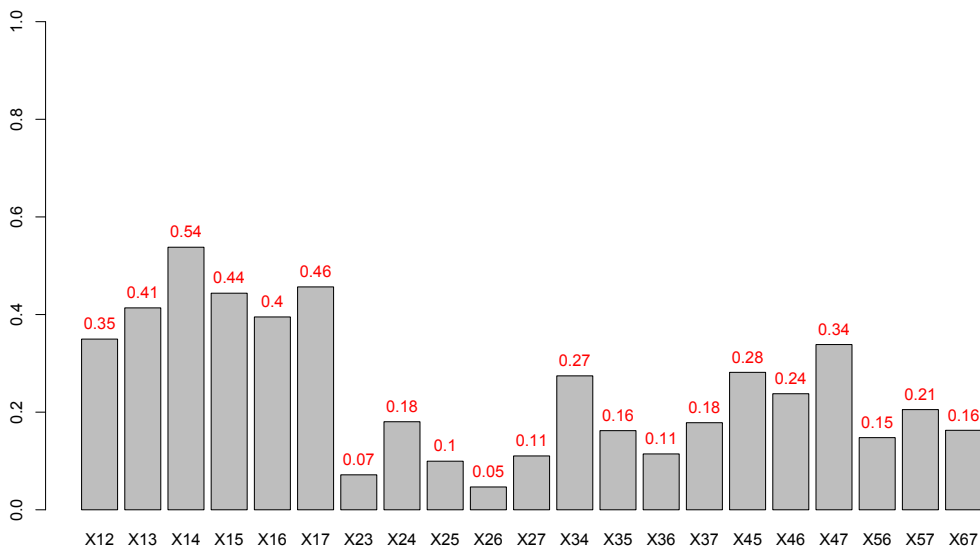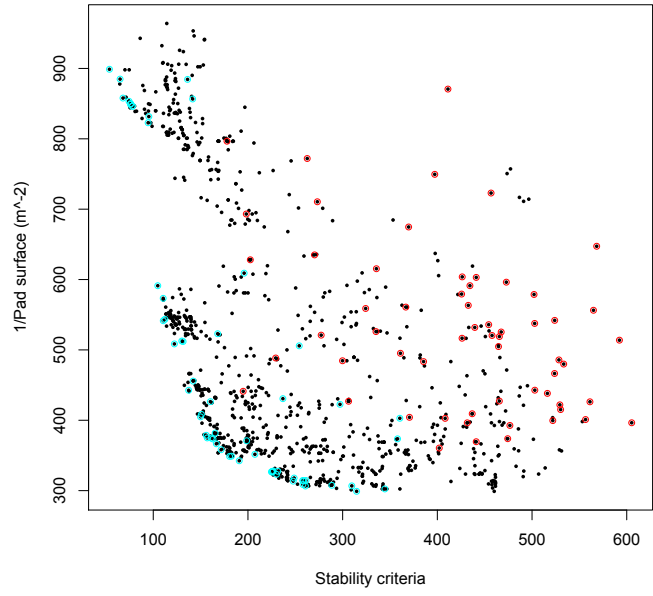
Figure 17: Closed second-order Sobol indices

Figure 18: Plot showing the Pareto front with red representing the initial generation and cyan for the final generation

List of Tables

	Disc (m)			Pad (m)			
	thickness	External radius	Internal radius	thickness	Internal radius	External radius	Angle (degree)
	$X1$	$X2$	$X3$	$X4$	$X5$	$X6$	$X7$
min	125.e-4	15.e-2	25.e-3	11.e-3	8.e-2	11.e-2	26
max	2.e-2	16.e-2	4.e-2	15.e-3	9.e-2	12.e-2	50

Table 1: Model: Parameter range considered

Location on the pareto front (approx.)	Disc (m) thickness X1	External radius X2	Internal radius X3	Pad (m) thickness X4	Internal radius X5	External radius X6	Angle (degree) X7	Optimization criteria	
								Stabilty criteria	Pad surface criteria
Upper left	156.e-4	157.e-3	292.e-4	144.e-4	872.e-4	11.e-2	26	62.76	947.57
Middle	126.e-4	158.e-3	269.e-4	141.e-4	85.e-3	118.e-3	48	192.94	353.23
Lower right	148.e-4	157.e-3	295.e-4	145.e-4	800.e-4	118.e-3	48	431.73	307.44

Table 2: Results of the Pareto front from three different locations